Enhancement of charge density wave correlations in a Holstein model with an anharmonic phonon potential

C. Kvande,[1,2,*] C. Feng,[3,2] F. Hébert,[4] G. G. Batrouni,[5,6,4] and R. T. Scalettar[2]

[1]*Physics Department, Kalamazoo College, 1200 Academy Street, Kalamazoo, Michigan, 49006-3295, USA*
[2]*Department of Physics, University of California, Davis, California 95616, USA*
[3]*Center for Computational Quantum Physics, Flatiron Institute, 162 Fifth Avenue, New York, New York 10010, USA*
[4]*Université Côte d'Azur, CNRS, INPHYNI, 17 rue Julien Lauprêtre, 06200 Nice, France*
[5]*Department of Physics, National University of Singapore, 2 Science Drive 3, 117551 Singapore*
[6]*Centre for Quantum Technologies, National University of Singapore; 2 Science Drive 3, 117543 Singapore*

(Received 4 April 2023; revised 4 July 2023; accepted 24 July 2023; published 7 August 2023)

The Holstein Hamiltonian describes itinerant electrons whose site density couples to local phonon degrees of freedom. In the single-site limit, at half filling, the electron-phonon coupling results in a double-well structure for the lattice displacement, favoring empty or doubly occupied sites. In two dimensions and on a bipartite lattice in $d \geqslant 2$, intersite hopping causes these doubly occupied and empty sites to alternate in a charge density wave (CDW) pattern when the temperature is lowered. Because a discrete symmetry is broken, this occurs in a conventional second-order transition at finite T_{cdw}. In this paper, we investigate the effect of changing the phonon potential energy to one with an *intrinsic* double-well structure even in the absence of electron-phonon coupling. While this aids in the initial process of pair formation, the implications for subsequent CDW order are nontrivial. One expects that, when the electron-phonon coupling is too strong, the double wells become deep and the polaron mass gets large, an effect which *reduces* T_{cdw}. We show here the existence of regions of parameter space where the double-well potential, while aiding local pair formation, does so in a way which also substantially enhances long-range CDW order.

DOI: 10.1103/PhysRevB.108.075119

I. INTRODUCTION

The Holstein Hamiltonian [1] provides a simplified description of the interactions between electron and phonon degrees of freedom in a solid, including polaron and bipolaron formation [2–10], and the origin of low-temperature phases with diagonal charge density wave (CDW) or off-diagonal superconducting (SC) long-range order [11–21]. Although the electron-phonon (*e*-ph) interaction λ initiates these phases, its effect is nonmonotonic [19,22–28]. Quantum Monte Carlo (QMC) simulations show that pairs become heavy and CDW and SC transition temperatures go to zero at strong coupling λ [29]. This finding is in contrast to the approximate Eliashberg theory, which predicts that T_{cdw} increases monotonically with λ and provides a challenge to achieving high CDW transition temperatures.

As a consequence, the search for situations in which large λ does not reduce the tendency for long-range order has been an ongoing focus of recent analytic and numerical studies. For example, in the case of superconductivity, it has been suggested that a Su-Schrieffer-Heeger (SSH) interaction [30–33] might avoid the problem of large effective mass [34,35]. Elevated CDW transitions have also been found in studies of the SSH model on a three-dimensional Lieb lattice appropriate to the bismuthates [36].

In infinite dimensions, using a technique similar to dynamical mean field theory (DMFT), Freericks *et al.* [37] studied the effects of a simple anharmonic term in the form of an additional quartic potential energy for the phonons. They concluded that a CDW phase exists for a large range of densities at low anharmonicity but that the CDW is gradually replaced at low and high densities by a SC phase as the anharmonicity increases. The half-filled system always remains in a CDW state. They also observed a decrease in the critical temperatures at which CDW and SC phases appear with increasing anharmonicity. Similar models have been studied in one dimension [38].

In this paper we consider a route to high CDW transition temperatures driven by a double-well (anharmonic) phonon potential resulting from *negative* quadratic and positive quartic terms in the displacement. Such a potential favors the development of a preexisting nonzero phonon field, without the mediation of electron-phonon coupling, and then favors electron occupations to organize into empty and doubly occupied sites when the *e*-ph interaction is present. A number of previous studies of anharmonicity with *positive* quadratic and positive quartic phonon potential energy terms [13,37–47] found, in general, a suppression of charge order at half filling, in agreement with the DMFT study noted above. Nonlinearities in the coupling terms between fermions and phonons [39–42] led to similar conclusions. This existing literature brings into focus our key result: Anharmonicity can produce an enhancement of T_{cdw} if it occurs in the form of an intrinsic double-well potential.

*Corresponding author: Claire.Kvande19@kzoo.edu

There are a number of experimental motivations for considering such a generalization of the Holstein Hamiltonian. One is to understand Kondo/heavy-fermion physics in materials like $SmOs_4Sb_{12}$. Most typically, heavy-fermion behavior arises due to the interaction of conduction electrons with *magnetic* degrees of freedom (local moments). However, it has been suggested, even dating back to Kondo [48], that other two-level systems might cause similar phenomena. In the case of $SmOs_4Sb_{12}$ a large applied magnetic field, which would quench fluctuations of local magnetic moments and hence of Kondo physics, does not destroy the heavy-fermion behavior. It has been suggested, then, that rather than conduction electrons interacting with local $S = 1/2$ spins, it is instead the coupling to two-level phonon degrees of freedom that is relevant [49,50].

The remainder of this paper is organized as follows: We first define the model, its parameters, and physical observables and then give a brief summary of our two complementary QMC techniques. Results are then shown for local observables and for charge structure factors for different forms of the anharmonic potential using energy scales close to those typically chosen in the conventional Holstein model. Finite-size scaling is employed to extract T_{cdw}. Similar calculations are then done for parameters which fix the average phonon displacement in order to demonstrate that the enhanced CDW T_{cdw} is not a "trivial" effect associated with artificially large displacements. A conclusion summarizes our work and points to possible future directions. The Appendixes contain further details of our model and simulations.

II. MODEL AND METHODS

We consider the Hamiltonian

$$\begin{aligned} H = &-t \sum_{\langle \vec{i}\,\vec{j}\rangle \sigma} (c^{\dagger}_{\vec{i}\sigma} c_{\vec{j}\sigma} + \mathrm{H.c.}) - \mu \sum_{\vec{i}\sigma} n_{\vec{i}\sigma} \\ &+ \sum_{\vec{i}} \left(-A x_{\vec{i}}^2 + B x_{\vec{i}}^4 + \frac{p_{\vec{i}}^2}{2m} \right) \\ &+ \lambda \sum_{\vec{i}} x_{\vec{i}} (n_{\vec{i}\uparrow} + n_{\vec{i}\downarrow} - 1). \end{aligned} \tag{1}$$

The sums run over the $N = L^2$ sites of a two-dimensional square lattice with periodic boundary conditions. The operator $c_{\vec{i}\sigma}$ ($c^{\dagger}_{\vec{i}\sigma}$) destroys (creates) a fermion of spin $\sigma = \uparrow$ or $\downarrow$ on site $\vec{i} = (i_x, i_y)$; $n_{\vec{i}\sigma} = c^{\dagger}_{\vec{i}\sigma} c_{\vec{i}\sigma}$ is the corresponding number operator, and $x_{\vec{i}}$ and $p_{\vec{i}}$ are the canonically conjugate displacement and momentum operators of the phonon mode at site $\vec{i}$. The first line of Eq. (1) represents the hopping energy of the fermions between neighboring sites $\langle \vec{i}, \vec{j} \rangle$. A chemical potential term is included to emphasize that our algorithms perform simulations in the grand canonical ensemble. The hopping parameter t will be used as the energy scale. The second line in Eq. (1) represents the energy of the phonons of the quadratic potential $-A x_{\vec{i}}^2$ and anharmonic term $B x_{\vec{i}}^4$. This form, with a negative quadratic term (i.e., $A > 0$), results in a double well. Without loss of generality, we set $m = 1$. The third line in Eq. (1) is the phonon-electron interaction, written in a particle-hole-symmetric (PHS) form so that $\mu = 0$ corresponds to half filling. Further discussion of this PHS appears in Appendix A. The PHS also ensures the values of displacement x corresponding to empty and doubly occupied sites are symmetrically located about the origin $x = 0$.

In order to connect to previous QMC studies of the conventional Holstein Hamiltonian [1], in which there is only a positive quadratic term in the phonon displacement with phonon frequency ω_0, we note that one would express the quadratic coefficient in terms of the frequency as $A = m\omega_0^2/2$. In that situation, ω_0 also enters the rewriting of the electron-phonon interaction in terms of phonon creation (destruction) operators $a^{\dagger}_{\vec{i}}$ ($a_{\vec{i}}$): $\lambda \sum_{\vec{i}} x_{\vec{i}} (n_{\vec{i}\uparrow} + n_{\vec{i}\downarrow} - 1) = g \sum_{\vec{i}} (a_{\vec{i}} + a^{\dagger}_{\vec{i}}) (n_{\vec{i}\uparrow} + n_{\vec{i}\downarrow} - 1)$, with $g = \lambda/\sqrt{2\omega_0}$, where $\omega_0 = \sqrt{2A}$. To make a comparison with previous work on the conventional Holstein model, we then choose a commonly used value of coupling g, keep B fixed to a small value, and vary A to explore different depths of the potential wells. The values of A are chosen to keep $\omega_0 = \sqrt{2A}$ and $\lambda = g\sqrt{2\omega_0}$ of order unity, in the range of values that are typically used for the conventional Holstein model. Results corresponding to this choice of parameters will be presented in Sec. III.

However, although analogous values of the e-ph coupling and phonon frequency are used in this comparison, the anharmonic form of the full phonon potential leads to displacements which are different in magnitude from the simplest harmonic situation. One can ensure that the coupling to the electrons, which combines λ and x_i, is equivalent in magnitude to the conventional Holstein case by choosing parameters A and B which are tuned to keep the average phonon displacement fixed at a certain value x_0, where x_0 is given by λ/ω_0^2 in the conventional Holstein case. This is accomplished through the choice $A = (4Bx_0^3 - \lambda)/(2x_0)$, a relation derived in Appendix B; results corresponding to this choice of parameters will be presented in Sec. IV.

We employ two methods to study Eq. (1). The first is determinant Quantum Monte Carlo (DQMC) [51]. In this approach, the action for the phonon degrees of freedom at inverse temperature (imaginary time) β is expressed as a path integral over a space-imaginary time grid, and the fermionic degrees of freedom, which appear only quadratically in Eq. (1), are integrated out analytically. The resulting partition function consists of an integral over the phonon field $x_{\vec{i}}(\tau)$ which is performed stochastically. The weight for phonon field configurations takes the form of the square of the determinant of a matrix (the fermionic traces over spin up and down yield identical determinants) whose dimension is the number of spatial sites N. Consequently, there is no sign problem. However, a sweep through the space-time lattice scales as $N^3\beta$ and possibly as $N^3\beta^2$, depending on the degree to which numerical instabilities require more accurate (numerically stable) treatment of the linear algebra.

DQMC studies of the conventional Holstein model date back to the same period as the Hubbard model [14,16,52–54], but precise quantitative values for T_{cdw} have emerged only more recently, e.g., on square [23], honeycomb [24], and cubic [28] lattices. The delay in computing the transition temperature originated partly because of the quantum simulation community's focus instead on electron-electron interactions as driving exotic superconductivity in cuprates

but also because of the significant computational challenge of very long autocorrelation times. In DQMC simulations of the Hubbard model, updates of the Hubbard-Stratonovich field at a single space-time point decorrelate very rapidly (a few sweeps of the lattice). However, in DQMC for the Holstein model, autocorrelation times are instead often hundreds or thousands of sweeps.

This bottleneck has led to the development of QMC methods for electron-phonon Hamiltonians based on a Langevin update of the entire space-time lattice [28,55–58]. Such approaches can be formulated in a way which scales linearly in N (albeit with a smaller step size for each move than in DQMC) via the replacement of the determinant by an integration over a pseudofermion field. Equally important to this linear scaling, Fourier acceleration methods [55,59] can be employed to reduce autocorrelation times dramatically. Quantitative details of DQMC and Langevin methods are discussed in Appendix C. Alternate methods to address long autocorrelation times use machine learning approaches [60] and Wang-Landau sampling [61].

We employ both the DQMC and Langevin methods here. Most of the simulations were performed with DQMC, and the results presented here were obtained with this method unless otherwise indicated in the figures. In certain key cases, results are confirmed by comparing DQMC and Langevin simulations.

The simplest observable we study is the density, $n = \sum_{\vec{i}} \langle n_{\vec{i}\sigma} \rangle / L^2$, and its behavior as a function of μ. A plateau in $n(\mu)$ signals a vanishing compressibility, $\kappa = \partial n / \partial \mu$, and the presence of a charge gap Δ. As noted earlier, the PHS form of the Hamiltonian ensures half filling $n = 1$ corresponds to $\mu = 0$. This is the optimal density for a CDW phase since it allows precise alternation of doubly occupied and empty sites.

We also examine other local quantities such as the average value of the phonon displacement $\langle x_{\vec{i}} \rangle$, the double occupancy $D = \langle n_{\vec{i}\uparrow} n_{\vec{i}\downarrow} \rangle$, and the x component of the kinetic energy $K = \langle c^{\dagger}_{\vec{i},\sigma} c_{\vec{i}+\hat{x},\sigma} + \text{H.c.} \rangle$.

To characterize further the presence of a (long-range) CDW phase, we study the charge structure factor, the Fourier transform at momentum (π, π) of the density-density correlation function,

$$S_{\text{cdw}} = \frac{1}{N} \sum_{\vec{i},\vec{j}} \langle n_{\vec{i}} n_{\vec{i}+\vec{j}} \rangle (-1)^{j_x + j_y} . \tag{2}$$

Here, $n_{\vec{i}} = n_{\vec{i}\uparrow} + n_{\vec{i}\downarrow}$ is the number of fermions on site $\vec{i}$. In a phase with short-range order, $\langle n_{\vec{i}} n_{\vec{i}+\vec{j}} \rangle$ will decay rapidly to zero as the separation $|\vec{j}|$ increases. Thus, in the sum over all sites $\vec{i}$ and separations $\vec{j}$ in Eq. (2), the only sizable contributions come from small separations $\vec{j}$, and the double sum is of order N. The division by N then implies $S_{\text{cdw}} \sim O(1)$, i.e., is independent of lattice size. In a phase with long-range order, on the other hand, the double sum is $O(N^2)$, and $S_{\text{cdw}} \sim O(N)$ (i.e., is extensive) after normalization. The optimal ordering vector $\vec{q}$ for a half-filled square lattice is at $\vec{q} = (\pi, \pi)$ owing to the perfect nesting at this momentum. Incommensurate order at $\vec{q} \neq (\pi, \pi)$ is possible upon doping, but we do not see evidence of it here.

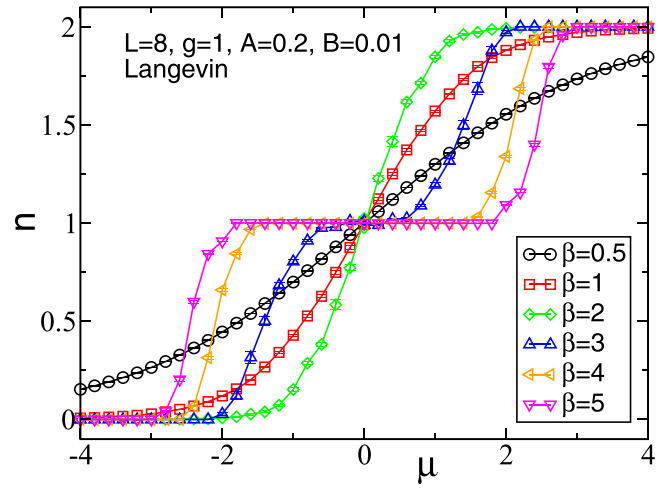

FIG. 1. Density n as a function of chemical potential μ for $g = 1$, $B = 0.01$, and $A = 0.2$. $\lambda = \sqrt{2\omega_0} g$, with $\omega_0 = \sqrt{2A}$. At high temperature T, n deviates immediately from half filling as μ is changed from $\mu = 0$. However, as T decreases, a plateau in $n(\mu)$ develops: the density is frozen at half filling until $|\mu|$ exceeds a critical threshold, half the single-particle gap Δ. This gap formation around $\beta \simeq 3$ is an indication of the entry into the ordered CDW phase at low T. The simulations were performed only for $\mu \geqslant 0$ since the system is particle-hole symmetric.

III. SIMULATIONS FOR CANONICAL PARAMETERS

We first show results for values of Hamiltonian parameters similar to those used in past studies of the conventional Holstein Hamiltonian in order to facilitate a comparison of our results with those in the literature. Specifically, we fix the electron-phonon coupling $g \sum_{\vec{i}} (a_{\vec{i}} + a^{\dagger}_{\vec{i}}) (n_{\vec{i}\uparrow} + n_{\vec{i}\downarrow} - 1)$ at $g = 1$ and pick $A = 0.1, 0.2, 0.5$. These values correspond to quadratic potential curvatures $\omega_0^2/2$ with $\omega_0 = \sqrt{2A} = 0.44, 0.63, 1.00$, similar to the commonly used values $\omega_0 = 0.5$–2.0 [19,22–28,40,41]. When expressed in terms of a coupling of fermionic density to lattice displacement, $\lambda = \sqrt{2\omega_0}\, g = 0.94, 1.12, 1.41$, again in the usual range of $\lambda \sim 1$.

A. Local observables

Phases with long-range order are typically characterized by gaps in their single-particle excitation spectra. As noted earlier, such gaps are most simply revealed via a vanishing of the compressibility $\kappa = \partial n / \partial \mu$, i.e., by a plateau in a plot of n versus μ. In Fig. 1 we fix $A = 0.2$, $B = 0.01$, and $g = 1$. At high temperatures the compressibility at half filling ($\mu = 0$) is finite. However, when $T \lesssim t/3$, the slope of $n(\mu = 0)$ becomes small. At $T = t/5$, n remains fixed at $n \sim 1$ until μ exceeds $\mu \sim 2t$, indicating a CDW gap $\Delta \sim 4t$. The nonmonotonic evolution of the compressibility in Fig. 1 can be understood by the fact that, in addition to the nontrivial physics of CDW formation which causes $\kappa \sim 0$ at low T, in the limit of very high temperature the compressibility must also become small, i.e., $\kappa \sim 1/T$.

Figure 2 generalizes Fig. 1 to several distinct values of A. As explained before, for each A, the electron-phonon coupling is chosen to mimic the procedure in the usual Holstein model, namely, by identifying the frequency corresponding to the

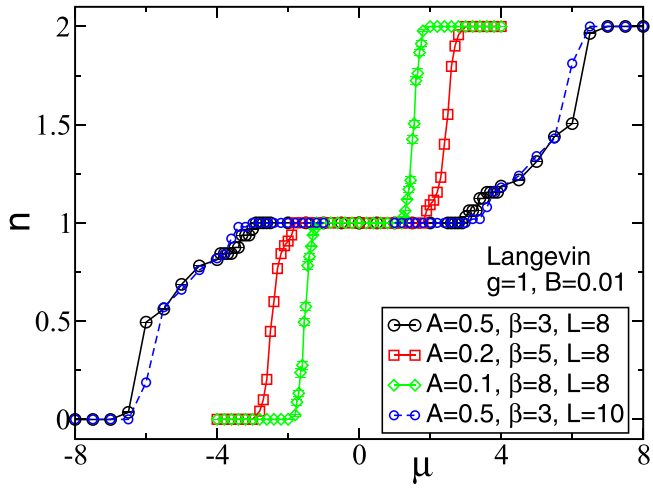

FIG. 2. Density n as a function of chemical potential μ for $g = 1$, $B = 0.01$, and several values of A with $\lambda = \sqrt{2\omega_0}g$ and $\omega_0 = \sqrt{2A}$. β is chosen so that $n(\mu)$ no longer changes with further lowering of the temperature, allowing the simulation to pick up only ground state properties. (See also Fig. 6.) We observe a decrease in the charge gap as A decreases from 0.5 to 0.1. For the $A = 0.5$ case, a comparison of results for $L = 8$ and $L = 10$ shows that the width of the gap does not change significantly with size.

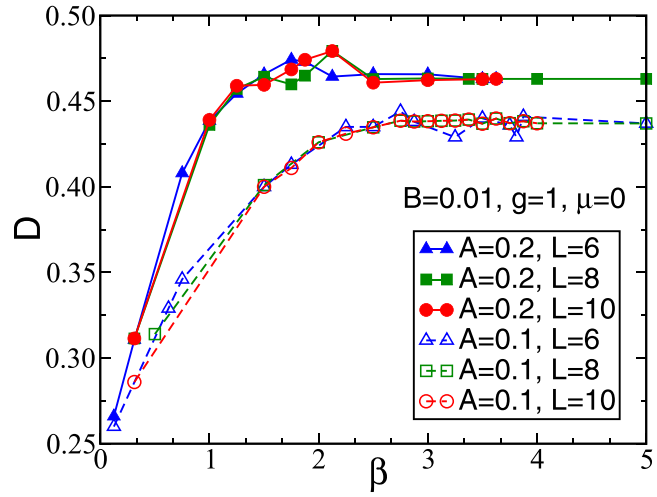

FIG. 3. The double occupancy D as a function of β for $B = 0.01$, $\mu = 0$, $g = 1$, different sizes L, and two different choices of A: $A = 0.1$ (open symbols and dashed lines) and $A = 0.2$ (solid symbols and solid lines). $\lambda = \sqrt{2\omega_0}g$, with $\omega_0 = \sqrt{2A}$. D saturates to a larger value and at a higher temperature for $A = 0.2$ compared to $A = 0.1$.

curvature, $\omega_0 = \sqrt{2A}$, and then determining the electron-phonon coupling $\lambda = \sqrt{2\omega_0}\, g$ with g fixed at $g = 1$. Figure 2 allows us to assess how the single-particle gap Δ is affected by the (negative) quadratic phonon curvature. We find that Δ increases with increasing A. We will return to this point in discussing the effect of varying A on the CDW transition temperature.

We comment that for $A = 0.5$, one can see additional steps in n above half filling. For $L = 8$ ($N = 64$), they occur at integer densities corresponding to even numbers of particles $N_\uparrow + N_\downarrow = 66, 68, \ldots$ on the lattice and reflect the tendency to add particles in $\uparrow\downarrow$ pairs due to the attractive interaction mediated by the phonons. Similar steps are evident for $L = 10$. This is an effect seen also in QMC simulations of the conventional Holstein model.

The double occupancy D is given in Fig. 3 for two values of A and different lattice sizes $L = 6, 8, 10$. D evolves rapidly from its high temperature (uncorrelated) value $D = \langle n_{\vec{i}\uparrow} n_{\vec{i}\downarrow}\rangle \sim \langle n_{\vec{i}\uparrow}\rangle \langle n_{\vec{i}\downarrow}\rangle \sim 1/4$ as T decreases, reflecting the fact that pair formation precedes the ordering of pairs into a CDW pattern. The weak feature in D at $\beta \sim 2$ will be seen to coincide with CDW formation.

A final local observable is the kinetic energy K, given in Fig. 4. K first evolves from its particle-hole-symmetric high-temperature limit $K = 0$ to negative values as lower-energy states dominate. This steady decrease is interrupted by upturns in K (decreases in the magnitude of hopping). These local maxima correlate with the CDW ordering transitions (see below).

B. Long-range charge order

Two final observables directly probe charge order. The first, shown in the top panel of Fig. 5, is the real-space density-density correlation function $\langle n_{\vec{i}}\, n_{\vec{i}+\vec{j}}\rangle$. At $\beta = 1$ it differs from its $\lambda = 0$ values $\langle n_{\vec{i}}\, n_{\vec{i}+\vec{j}}\rangle = \langle n_{\vec{i}}\rangle \langle n_{\vec{i}+\vec{j}}\rangle = 1$ only on site, $\vec{i} = \vec{j}$. That is, pairs have formed locally but have not yet ordered between different sites. However, at $\beta = 4$ the oscillating and nondecaying pattern indicates long-range CDW formation. Figure 6 exhibits the Fourier transform of Eq. (2), i.e., the structure factor $S_{\rm cdw}$. An additional normalization to $N = L^2$ is performed, so that $S_{\rm cdw}/N \propto 1/N$ at small

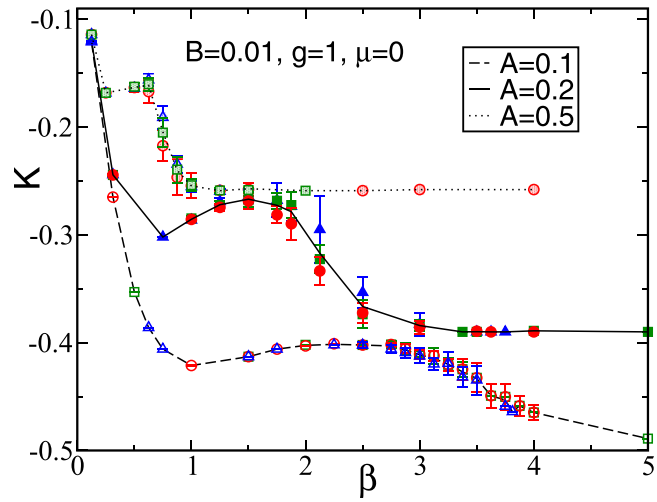

FIG. 4. K, the x component of kinetic energy, as a function of inverse temperature for different values of A, $A = 0.1$, 0.2, and 0.5, and different sizes $L = 6$, 8, and 10. All data have $B = 0.01$, $\mu = 0$, and $g = 1$. $\lambda = \sqrt{2\omega_0}g$, with $\omega_0 = \sqrt{2A}$. Red circles show $L = 10$, green squares show $L = 8$, and blue triangles show $L = 6$. The lines show the average over the different lattice sizes at each point. Because of particle-hole symmetry, the high-temperature (small-β) value of K vanishes: The noninteracting energy levels $\epsilon(\mathbf{k})$ are symmetric around $\epsilon = 0$, and at high T, all levels are occupied equally. As β increases, the $\epsilon < 0$ states are preferentially occupied, and $K < 0$.

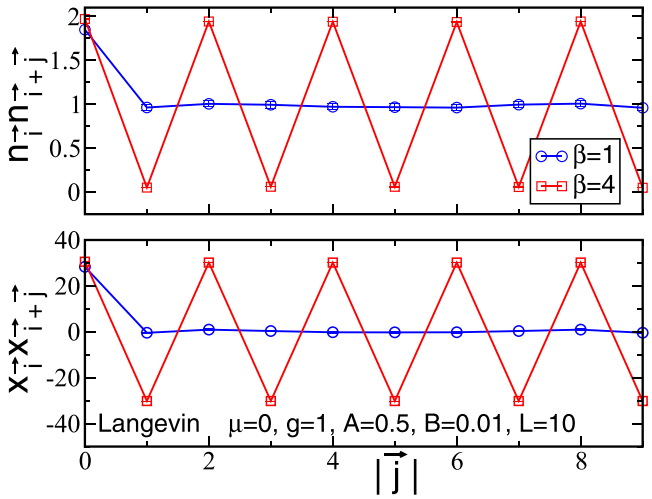

FIG. 5. Density-density $\langle n_{\vec{i}} n_{\vec{i}+\vec{j}} \rangle$ and phonon displacement $\langle x_{\vec{i}} x_{\vec{i}+\vec{j}} \rangle$ correlators along the side of the square lattice at high ($\beta = 1$) and low ($\beta = 4$) temperatures at $\mu = 0$ (half filling). As β increases, the system goes from an unordered phase to a charge density wave phase where an order develops in both the charge density and phonon displacements. One should notice that, for $\vec{j} = \vec{0}$, due to the double-well potential, $\langle x_{\vec{i}} x_{\vec{i}} \rangle$ is sizable even in the high-temperature phase.

β, and $S_{\rm cdw}/N \propto 1$ at large β. An abrupt change indicates the CDW transition. The invariance of the low-T value across different lattice sizes is another indication the order is long range.

The positions of these steps are close to the locations of the local minima in the absolute value of the kinetic energy K in Fig. 4. We interpret this to indicate that the preferential occupation of bands with $\epsilon(\mathbf{k}) < 0$, which occurs even in the noninteracting limit as T is lowered, gets interrupted by the CDW formation.

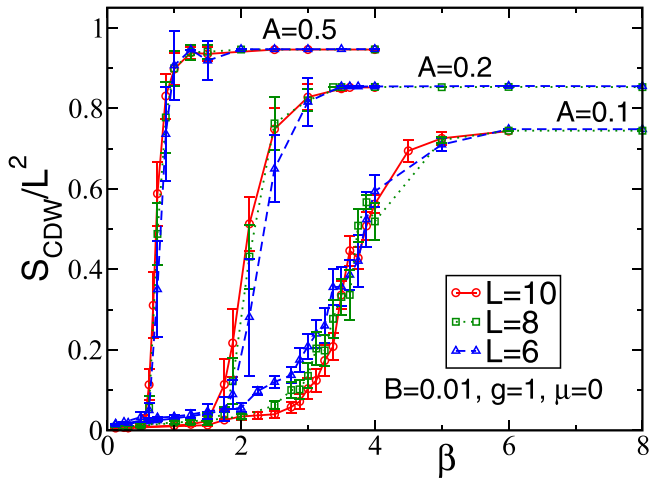

FIG. 6. Evolution of the charge structure factor $S_{\rm cdw}$ with inverse temperature. Here, $B = 0.01$, $\mu = 0$, and $g = 1$. From left to right, we have $A = 0.5$, $A = 0.2$, and $A = 0.1$ with corresponding $\omega_0 = \sqrt{2A}$ and $\lambda = \sqrt{2\omega_0} g$. As A increases, the structure factor $S_{\rm cdw}$ saturates at a larger value, and the transition occurs at a larger temperature.

The bottom panel of Fig. 5 indicates that the alternating pattern in the fermionic density is accompanied by an alternating pattern in the phonon displacements.

The key features of Fig. 6, however, are the *high values of the transition temperatures* $T_{\rm cdw}$ for the larger values of A where the double-well phonon potential energy favors nonzero displacements. Typical values of $T_{\rm cdw}$ in the conventional Holstein model are in the range $T_{\rm cdw}/t \sim 0.2$–0.3 for analogous choices of g and ω_0 [25]. In the next section, we verify that these high $T_{\rm cdw}$ persist even when the product of the electron-phonon coupling and typical phonon displacements are restricted to be the same as in the conventional Holstein model.

We conclude this discussion by presenting a scaling analysis to determine $T_{\rm cdw}$ more precisely. When normalized by $N^{-1} = L^{-2}$, a lattice-size-independent structure factor provides evidence for ground state long-range order, as already seen in Fig. 6. The temperature at which this order first occurs can be determined by examining $L^{-\gamma/\nu} S_{\rm cdw}$. The theory of finite-size scaling predicts that curves of $L^{-\gamma/\nu} S_{\rm cdw}$ as functions of T (or β) for different lattice sizes should all cross at one point, thus yielding the value of $T_{\rm cdw}$. Here, in the Holstein model on a square lattice, the transition is in the two-dimensional (2D) Ising universality class with $\gamma/\nu = 7/4$, simplifying the analysis. Figure 7 shows the result for the two cases with $A = 0.1$ (top) and $A = 0.5$ (bottom). The crossing is at $T_{\rm cdw} = 0.29 \pm 0.02$ ($\beta_{\rm cdw} = 3.5 \pm 0.2$) for $A = 0.1$ and as high as $T_{\rm cdw} = 1.8 \pm 0.2$ ($\beta_{\rm cdw} = 0.56 \pm 0.06$) for $A = 0.5$.

We also demonstrate that the two computational methods, DQMC and Langevin, give consistent results by comparing results for $L = 8$ in the insets of Fig. 7.

IV. SIMULATIONS AT FIXED AVERAGE PHONON DISPLACEMENT

In the preceding section we reported values for $T_{\rm cdw}/t$ which exceed by a factor of 2 or 3 those obtained over a range of values of electron-phonon couplings λ and phonon frequencies ω_0 previously reported for the conventional Holstein Hamiltonian.

These results are already significant because the existence of a maximal $T_{\rm cdw}/t$ at intermediate λ and ω_0 suggests a fundamental limit to the CDW transition temperature in the conventional Holstein model. However, one could still ask whether the high critical transition temperatures of Fig. 6 are associated with anomalously large phonon displacements or some related unphysical parameter choice. In this section we reproduce many of the preceding results tuning the anharmonic potential (that is, A and B) to keep fixed phonon displacement. More specifically, we show in Appendix B that the choice

$$A = \frac{4Bx_0^3 - \lambda}{2x_0} \tag{3}$$

keeps $\langle x \rangle = x_0$. Thus, when we vary A, we do so with an accompanying change in B to fix the mean phonon displacement. We choose to compare our results to the conventional Holstein model with $\lambda = 2$ and $\omega_0 = 1$, for which $x_0 = \langle x \rangle = \lambda/\omega_0^2 = 2$. In addition, we use the same value of $\lambda = 2$ in

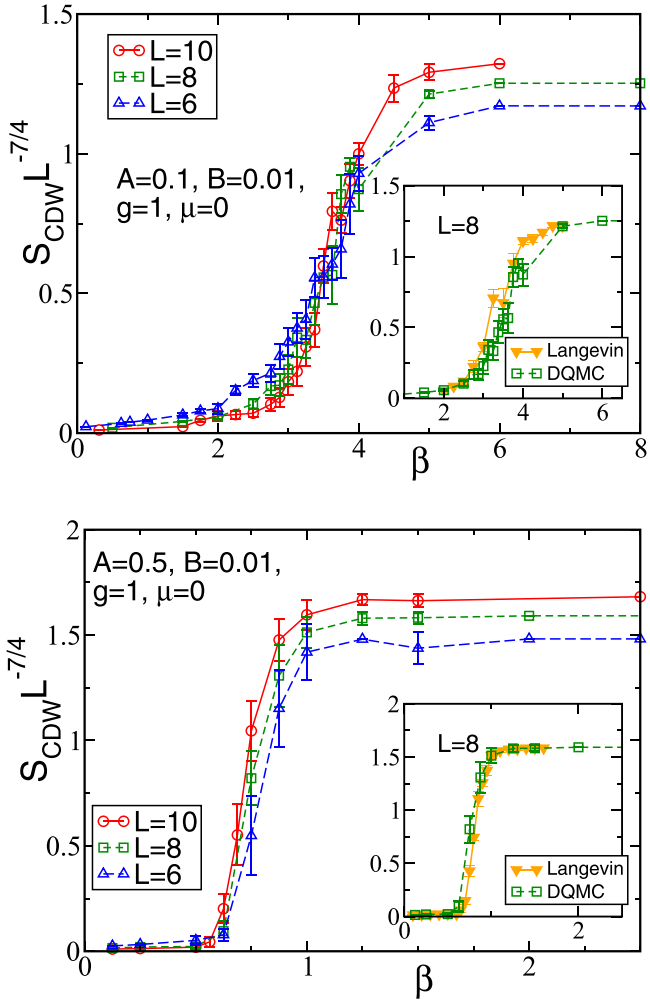

FIG. 7. Scaling analysis of the charge structure factor for $B = 0.01$, $g = 1$, $\mu = 0$, and $A = 0.1$ (top) or $A = 0.5$ (bottom) with corresponding $\omega_0 = \sqrt{2A}$ and $\lambda = \sqrt{2\omega_0}g$. When $S_{\rm cdw}$ is normalized by $L^{\gamma/\nu}$ with $\gamma/\nu = 7/4$, the 2D Ising values, a crossing that is a function of inverse temperature β occurs at the critical point. The top panel shows the $A = 0.1$ case for which we observe the crossing around $\beta_{\rm cdw} = 3.5 \pm 0.2$. In the bottom panel, $A = 0.5$, and $\beta_{\rm cdw} = 0.56 \pm 0.06$. The insets show a comparison between results obtained with DQMC and Langevin methods for $L = 8$ in the critical region.

both models to keep the products λx similar. We study cases with $B = 0.1$ and $B = 0.2$, which give $A = 0.3$ and $A = 1.1$, respectively.

A. Local observables

To ensure the observation of the high CDW transition temperatures reported in the preceding section is robust, we focus here on measurements of long-range order which more precisely determine $T_{\rm cdw}$. Nevertheless, it is useful to examine one local measurement, the kinetic energy, since its nonmonotonic behavior was seen earlier to provide an important initial indication of the onset of the insulating CDW phase. Figure 8 exhibits this decrease in the magnitude of K in the vicinity of the CDW ordering transition.

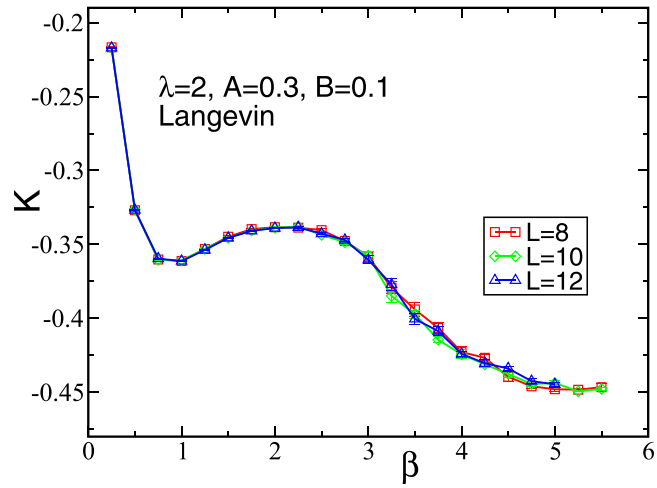

FIG. 8. Kinetic energy as a function of β. The nonmonotonic behavior of the kinetic energy reflects the development of charge correlations. Parameters are $A = 0.3$, $B = 0.1$, and $\lambda = 2$ and were chosen to obtain a phonon field $x_0 = 2$.

B. Long-range charge order

Figure 9 shows a finite-size scaling crossing plot for these "fair comparisons" in which the phonon displacement is restricted to be the same as for the conventional Holstein model. We find $\beta_{\rm cdw} \sim 3.25$ ($T_{\rm cdw} \sim 0.31$), which is higher than the transition temperature of the Holstein model on a half-filled square lattice with $\lambda = 2, \omega_0 = 1$ [26]. Choosing $A = 1.1$ and $B = 0.2$ and keeping $\lambda = 2$, $\omega_0 = 1$, and $x_0 = 2$, we increase the transition temperature to $\beta_{\rm cdw} = 2.5$. This shows that for the same fixed average value of lattice displacement x_0, we obtain higher critical temperatures by increasing A and B. Furthermore, as noted earlier, $T_{\rm cdw}$ as a function

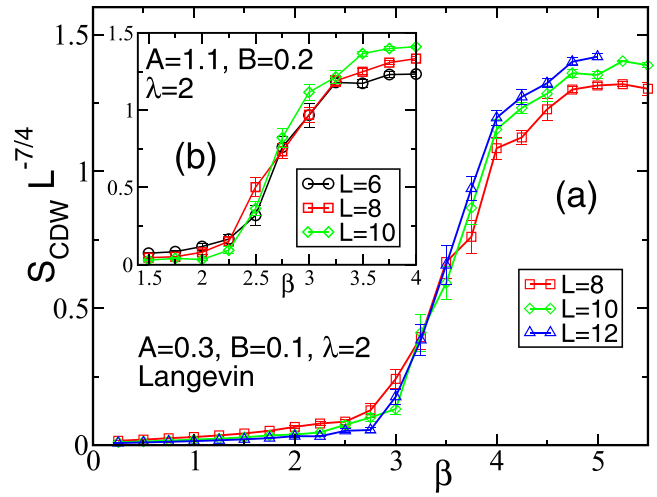

FIG. 9. Langevin data for the rescaled structure factor $S_{\rm cdw}L^{-7/4}$ for (a) $A = 0.3$, $B = 0.1$, and $\lambda = 2$ and (b) $A = 1.1$, $B = 0.2$, and $\lambda = 2$. Both cases correspond to a phonon field $x_0 = 2$. A crossing at $\beta_{\rm cdw} \sim 3.25$ in (a) gives the position of the CDW transition for $A = 0.3$ and $B = 0.1$, whereas the transition is shifted towards $\beta_{\rm cdw} \sim 2.5$ for $A = 1.1$ and $B = 0.2$ in (b). One should notice that our simulations are limited to $L = 10$ for the second case.

of λ in the Holstein model is nonmonotonic, with a maximum $T_{\rm cdw} \sim 0.25$ at dimensionless electron-phonon coupling strength $\lambda_D \sim 0.4$ when $\omega_0 = 1$ [26]. Meanwhile, the transition temperature does not depend on ω_0 sensitively as long as the effective attraction in the Holstein model $U = -\lambda^2/\omega_0^2$ is fixed [58]. The large $T_{\rm cdw} \sim 2$ shown in Fig. 7 (bottom), much higher than the maximum $T_{\rm cdw}$ we can achieve in the pure Holstein model, indicates that the Holstein model with anharmonic potential we study here significantly increases the CDW phase transition temperature.

V. CONCLUSIONS

In this paper we have used determinant Quantum Monte Carlo and Langevin simulations to examine the properties of a square lattice Holstein model with an anharmonic phonon potential. This potential has an intrinsic double-well structure favoring nonzero phonon fields and, consequently, empty and doubly occupied sites. Unlike most previous extensions of the Holstein model to include anharmonicity, our results show a marked increase in the CDW transition temperatures, from $T_{\rm cdw} \sim t/6$–$t/4$ for the conventional Holstein model to $T_{\rm cdw} \sim t/2$–t. Our result is not a consequence of a trivial rescaling of $T_{\rm cdw}$ resulting from larger phonon displacements; we demonstrated this by choosing parameter sets in which the average phonon displacement is similar to those in the conventional Holstein model. In any case, in the Holstein-Hubbard model, $T_{\rm cdw}$ has a maximum that is a function of electron-phonon coupling, phonon frequency, and the resulting phonon displacement, which is well below the transition temperatures found here.

It would be interesting to explore superconducting correlations in this model. One expects the CDW and superconductivity to be competitive, so that the emergence of superconductivity will surely require doping away from half filling. QMC is especially useful here, especially given the uncertainty in how to include anharmonicity [46] in analytic approaches like Migdal-Eliashberg theory [62,63], which have been central to the understanding of the conventional Holstein Hamiltonian [29,42,64,65]. Progress has been made in that method by generalizing the single-phonon spectral density [46].

Although we have mainly characterized our CDW phase as one in which the electron density is modulated, there is an accompanying alternation of phonon coordinates in our model, as seen in the bottom panel of Fig. 5. Since our phonon degrees of freedom are not directly coupled to each other, this oscillating structure forms via coupling to the conduction electrons. This effect is similar to that occurring in the dense limit of the Kondo lattice model [66–68], in which local moments which have no direct coupling can, nevertheless, order antiferromagnetically via an indirect Ruderman-Kittel-Kasuya-Yosida [69–71] interaction mediated by conduction electrons.

A potentially interesting application of the use of QMC to compute the properties of anharmonic electron-phonon systems is to study the physics of "rattlers" for high-figure-of-merit thermoelectric materials, specifically the thermal conductivity [72,73].

ACKNOWLEDGMENTS

The work of R.T.S. was supported by Grant No. DE-SC0014671 funded by the U.S. Department of Energy, Office of Science. C.K.'s work was supported by the University of California, Davis, Physics REU program under NSF Grant No. PHY2150515.

APPENDIX A: PARTICLE-HOLE SYMMETRY IN THE PRESENCE OF AN ANHARMONIC POTENTIAL

There are two related ways to discuss the particle-hole symmetry of the model. As the one-particle band due to the kinetic term is symmetric around $\mu = 0$, the first way is to consider a single-site model (that is, $t = 0$) with the phonon potential of Eq. (1),

$$V(x) = -Ax^2 + Bx^4 + \lambda x(n-1) - \mu n, \tag{A1}$$

and to show it has a similar particle-hole symmetry.

The average density is given by

$$\langle n_\uparrow \rangle = Z^{-1} \sum_{n_\uparrow=0}^{1} \sum_{n_\downarrow=0}^{1} \int dx\, n_\uparrow\, e^{-\beta V(x)},$$

$$Z = \sum_{n_\uparrow=0}^{1} \sum_{n_\downarrow=0}^{1} \int dx\, e^{-\beta V(x)}. \tag{A2}$$

If we introduce the notation $I(n_\uparrow, n_\downarrow)$ to denote the integral for a specific choice of number operators, we can rewrite Eq. (A2) as

$$\langle n_\uparrow \rangle = \frac{I(1,0) + I(1,1)}{I(0,0) + 2I(1,0) + I(1,1)}, \tag{A3}$$

where the denominator is the partition function. Rearranging this shows that the half-filling condition $\langle n_\uparrow \rangle = 1/2$ is $I(0,0) = I(1,1)$, which can be true only when $\mu = 0$. When $\mu = 0$, the curves of $V(x)$ for $n = 0$ and $n = 2$ are reflections of each other in the y axis, thus giving us symmetry between the "hole" and "particle" curves.

A more formal analysis is to apply a particle-hole transformation (PHT), $d_{\vec{i}\sigma} = (-1)^{i_x+i_y} c^\dagger_{\vec{i}\sigma}$, on the Hamiltonian. This choice of alternating signs between different sublattices sites ensures that the electron hopping term remains the same under the PHT. Meanwhile, the density operator $n_{\vec{i}\sigma}$ transforms into $1 - n_{\vec{i}\sigma}$. If we also introduce $y_{\vec{i}} = -x_{\vec{i}}$, we see that the original Hamiltonian is recovered except for a change in sign of the chemical potential μ. This demonstrates that density of the system obeys $n(\mu) = 2 - n(-\mu)$. From this, it is obvious that $\mu = 0$ yields half filling $n = \langle n_{\vec{i}\uparrow} + n_{\vec{i}\downarrow} \rangle = 1$.

APPENDIX B: RELATION BETWEEN A AND B TO FIX x_0

In order to compare the results of simulations of the anharmonic model to the original Holstein Hamiltonian, setting the e-ph coupling λ and phonon frequency ω_0 (with $\omega_0 = \sqrt{2A}$) to be the same, as done in Sec. III, is not sufficient. The reason is that the electrons move in an energy landscape given by the *product* of λ and phonon displacement. A comparison which ensures equivalence of the energy landscape is obtained by requiring that λx_0 be the same in the double-well potential as in the conventional Holstein model. Here, x_0 is the position of

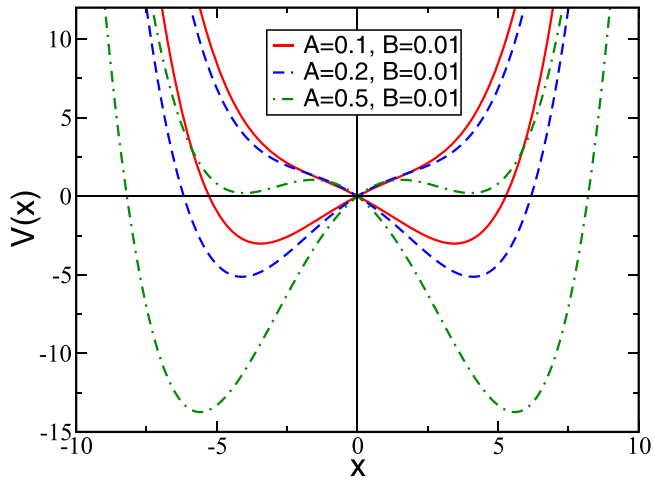

FIG. 10. Plots of $V(x) = -Ax^2 + Bx^4 + \lambda x(n-1)$ for $n = 0$ and $n = 2$ for $(A, B) = (0.1, 0.01)$ (red solid lines), $(0.2, 0.01)$ (blue dashed lines), and $(0.5, 0.01)$ (green dot-dashed lines). Here, $\lambda = \sqrt{2\omega_0 g}$, where $\omega_0 = \sqrt{2A}$ and $g = 1$.

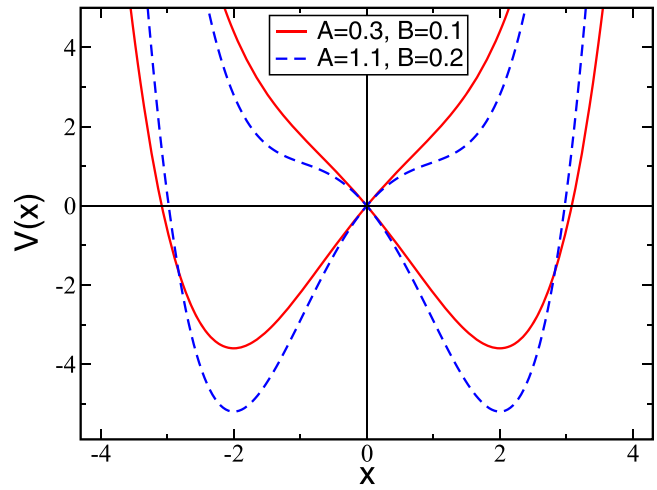

FIG. 11. Plots of $V(x) = -Ax^2 + Bx^4 + \lambda x(n-1)$ for $n = 0$ and $n = 2$ for $(A, B) = (0.3, 0.1)$ (red solid lines) and $(1.1, 0.2)$ (blue dashed lines). Here, $\lambda = 2$, and $\omega_0 = 1$, giving $x_0 = 2$ for both parameter sets.

the minima in the phonon potential corresponding to empty ($n = 0$) and doubly occupied ($n = 2$) sites.

In the conventional Holstein Hamiltonian, at half filling ($\mu = 0$)

$$V = \tfrac{1}{2}\omega_0^2 x^2 + \lambda x(n-1), \tag{B1}$$

and the minima are at $x_0 = \pm\lambda/\omega_0^2$ for $n = 0$ and $n = 2$, respectively. It is straightforward to determine A and B in the anharmonic double-well potential to give the same x_0. The phonon potential is given by Eq. (A1) with $\mu = 0$ at half filling. The minimum of the $n = 0$ curve is at positive x_0 (the minimum for $n = 2$ is at $-x_0$) and is given by the condition

$$-2Ax_0 + 4Bx_0^3 - \lambda = 0. \tag{B2}$$

Therefore, to keep the locations of the minima fixed, A and B must satisfy

$$A = \frac{4Bx_0^3 - \lambda}{2x_0}. \tag{B3}$$

In addition, one should use the same value of λ in both models so that the product λx_0 is the same. Thus, in Sec. IV we proceed by fixing a (small) B and using Eq. (B3) to determine A. Commonly used parameters are, for example, $\lambda = 2$ and $\omega_0 = 1$, which yield $x_0 = 2$. We used these parameters for comparison. We note that the height of the barrier at x_0 between the minima is given by $Ax_0^2 + Bx_0^4 - \lambda x_0$.

APPENDIX C: COMPARISON OF DQMC AND LANGEVIN METHODS

The determinant quantum Monte Carlo (DQMC) and Langevin QMC algorithms differ in how they sample the fermion determinant. The partition function of the system is given by

$$Z = \mathrm{Tr}e^{-\beta H} \tag{C1}$$

$$= \mathrm{Tr}e^{-\Delta\tau H}e^{-\Delta\tau H}\cdots e^{-\Delta\tau H}, \tag{C2}$$

where H is given by Eq. (1) and $\Delta\tau$ is the imaginary time step, $\beta \equiv L_\tau \Delta\tau$. Complete sets of phonon coherent states $\{x_{\vec{i},\tau}\}$ are inserted at each imaginary time slice, which then allows us to express the trace over the phonon operators as a path integral. In addition, since the fermion operators appear only in quadratic form, they can be traced out, leading to the well-known expression [51]

$$\mathcal{Z} = \int \mathcal{D}x_{\vec{i},\tau} e^{-S_{\mathrm{ph}}} [\det M(\{x_{\vec{i},\tau}\})]^2, \tag{C3}$$

where the "phonon action" is

$$S_{\mathrm{ph}} = \frac{\Delta\tau}{2}\left[\omega^2 \sum_{\vec{i}} x_{\vec{i},\tau}^2 + \sum_{\vec{i}} \left(\frac{x_{\vec{i},\tau+1} - x_{\vec{i},\tau}}{\Delta\tau}\right)^2\right]. \tag{C4}$$

In DQMC, the statistical weight, the integrand in Eq. (C3), is sampled directly by using the Metropolis update scheme: every site is visited, and an attempt is made to change the phonon variable there. The attempted change is accepted or rejected using the Metropolis criterion [74]. In the Langevin approach [55], the partition function is first written as

$$\mathcal{Z} = \int \mathcal{D}x_{\vec{i},\tau} e^{-S}, \tag{C5}$$

where

$$S = S_{\mathrm{ph}} - \ln(\det M)^2. \tag{C6}$$

Now the phonon field $\{x_{\vec{i},\tau}\}$ is evolved using the Langevin equation, which, in the simplest Euler discretized time form, is given by [55]

$$x_{\vec{i},\tau,t+dt} = x_{\vec{i},\tau,t} - dt\frac{\partial S}{\partial x_{\vec{i},\tau,t}} + \sqrt{2\,dt}\,\eta_{\vec{i},\tau,t}, \tag{C7}$$

where t is the Langevin time and η is a Gaussian distributed stochastic variable. In practice we use higher-order Runge-Kutta discretization, and because the entire field is updated in one time step, we also use Fourier acceleration [55], which greatly reduces critical slowing down, speeding up the convergence of configurations to equilibrium. Fourier acceleration

cannot be used with DQMC because the field is updated one site at a time.

For more technical details, see Refs. [51,75,76] for DQMC and Ref. [55] for Langevin.

APPENDIX D: VISUALIZATION OF ANHARMONIC POTENTIALS

Throughout this paper, we discussed results from five different choices of parameters A and B of the anharmonic potential given in Eq. (A1) at $\mu = 0$. The first three choices, for commonly used parameters, are shown in Fig. 10. For visual simplicity, we show only the $n = 0$ and $n = 2$ curves for each parameter set.

We also show in Fig. 11 the two potentials for the parameters that fix the average phonon displacement. Again, only the $n = 0$ and $n = 2$ curves are shown for each parameter set. The minima are aligned, showing that x_0 is fixed at 2.

[1] Th. Holstein, Studies of polaron motion: Part I. The molecular-crystal model, Ann. Phys. (NY) **8**, 325 (1959).

[2] P. E. Kornilovitch, Continuous-Time Quantum Monte Carlo Algorithm for the Lattice Polaron, Phys. Rev. Lett. **81**, 5382 (1998).

[3] P. E. Kornilovitch, Ground-state dispersion and density of states from path-integral Monte Carlo: Application to the lattice polaron, Phys. Rev. B **60**, 3237 (1999).

[4] A. S. Alexandrov, Polaron dynamics and bipolaron condensation in cuprates, Phys. Rev. B **61**, 12315 (2000).

[5] M. Hohenadler, H. G. Evertz, and W. von der Linden, Quantum Monte Carlo and variational approaches to the Holstein model, Phys. Rev. B **69**, 024301 (2004).

[6] L.-C. Ku, S. A. Trugman, and J. Bonča, Dimensionality effects on the Holstein polaron, Phys. Rev. B **65**, 174306 (2002).

[7] P. E. Spencer, J. H. Samson, P. E. Kornilovitch, and A. S. Alexandrov, Effect of electron-phonon interaction range on lattice polaron dynamics: A continuous-time quantum Monte Carlo study, Phys. Rev. B **71**, 184310 (2005).

[8] A. Macridin, G. A. Sawatzky, and M. Jarrell, Two-dimensional Hubbard-Holstein bipolaron, Phys. Rev. B **69**, 245111 (2004).

[9] A. H. Romero, D. W. Brown, and K. Lindenberg, Effects of dimensionality and anisotropy on the Holstein polaron, Phys. Rev. B **60**, 14080 (1999).

[10] J. Bonča, S. A. Trugman, and I. Batistić, Holstein polaron, Phys. Rev. B **60**, 1633 (1999).

[11] R. E. Peierls, *Surprises in Theoretical Physics*, Princeton Series in Physics, Vol. 107 (Princeton University Press, Princeton, NJ, 1979).

[12] J. E. Hirsch and E. Fradkin, Effect of Quantum Fluctuations on the Peierls Instability: A Monte Carlo Study, Phys. Rev. Lett. **49**, 402 (1982).

[13] J. E. Hirsch and E. Fradkin, Phase diagram of one-dimensional electron-phonon systems. II. The molecular-crystal model, Phys. Rev. B **27**, 4302 (1983).

[14] R. T. Scalettar, N. E. Bickers, and D. J. Scalapino, Competition of pairing and Peierls–charge-density-wave correlations in a two-dimensional electron-phonon model, Phys. Rev. B **40**, 197 (1989).

[15] F. Marsiglio, Pairing and charge-density-wave correlations in the Holstein model at half-filling, Phys. Rev. B **42**, 2416 (1990).

[16] J. K. Freericks, M. Jarrell, and D. J. Scalapino, Holstein model in infinite dimensions, Phys. Rev. B **48**, 6302 (1993).

[17] T. Ohgoe and M. Imada, Competition among Superconducting, Antiferromagnetic, and Charge Orders with Intervention by Phase Separation in the 2D Holstein-Hubbard Model, Phys. Rev. Lett. **119**, 197001 (2017).

[18] M. Hohenadler and G. G. Batrouni, Dominant charge density wave correlations in the Holstein model on the half-filled square lattice, Phys. Rev. B **100**, 165114 (2019).

[19] O. Bradley, G. G. Batrouni, and R. T. Scalettar, Superconductivity and charge density wave order in the two-dimensional Holstein model, Phys. Rev. B **103**, 235104 (2021).

[20] B. Nosarzewski, E. W. Huang, P. M. Dee, I. Esterlis, B. Moritz, S. A. Kivelson, S. Johnston, and T. P. Devereaux, Superconductivity, charge density waves, and bipolarons in the Holstein model, Phys. Rev. B **103**, 235156 (2021).

[21] M. V. Araújo, J. P. de Lima, S. Sorella, and N. C. Costa, Two-dimensional $t - t'$ Holstein model, Phys. Rev. B **105**, 165103 (2022).

[22] S. Blawid and A. J. Millis, Quantum phonons and the charge-density-wave transition temperature: A dynamical mean-field study, Phys. Rev. B **63**, 115114 (2001).

[23] M. Weber and M. Hohenadler, Two-dimensional Holstein-Hubbard model: Critical temperature, Ising universality, and bipolaron liquid, Phys. Rev. B **98**, 085405 (2018).

[24] Y.-X. Zhang, W.-T. Chiu, N. C. Costa, G. G. Batrouni, and R. T. Scalettar, Charge Order in the Holstein Model on a Honeycomb Lattice, Phys. Rev. Lett. **122**, 077602 (2019).

[25] C. Feng, H. Guo, and R. T. Scalettar, Charge density waves on a half-filled decorated honeycomb lattice, Phys. Rev. B **101**, 205103 (2020).

[26] C. Feng and R. T. Scalettar, Interplay of flat electronic bands with Holstein phonons, Phys. Rev. B **102**, 235152 (2020).

[27] C. Chen, X. Y. Xu, Z. Y. Meng, and M. Hohenadler, Charge-Density-Wave Transitions of Dirac Fermions Coupled to Phonons, Phys. Rev. Lett. **122**, 077601 (2019).

[28] B. Cohen-Stead, K. Barros, Z. Y. Meng, C. Chen, R. T. Scalettar, and G. G. Batrouni, Langevin simulations of the half-filled cubic Holstein model, Phys. Rev. B **102**, 161108(R) (2020).

[29] I. Esterlis, S. A. Kivelson, and D. J. Scalapino, A bound on the superconducting transition temperature, npj Quantum Mater. **3**, 59 (2018).

[30] B. Xing, W.-T. Chiu, D. Poletti, R. T. Scalettar, and G. Batrouni, Quantum Monte Carlo Simulations of the 2D Su-Schrieffer-Heeger Model, Phys. Rev. Lett. **126**, 017601 (2021).

[31] C. Feng, B. Xing, D. Poletti, R. Scalettar, and G. Batrouni, Phase diagram of the Su-Schrieffer-Heeger-Hubbard model on a square lattice, Phys. Rev. B **106**, L081114 (2022).

[32] A. Götz, S. Beyl, M. Hohenadler, and F. F. Assaad, Valence-bond solid to antiferromagnet transition in the two-dimensional Su-Schrieffer-Heeger model by Langevin dynamics, Phys. Rev. B **105**, 085151 (2022).

[33] X. Cai, Z.-X. Li, and H. Yao, Antiferromagnetism Induced by Bond Su-Schrieffer-Heeger Electron-Phonon Coupling: A Quantum Monte Carlo Study, Phys. Rev. Lett. **127**, 247203 (2021).
[34] J. Sous, M. Chakraborty, R. V. Krems, and M. Berciu, Light Bipolarons Stabilized by Peierls Electron-Phonon Coupling, Phys. Rev. Lett. **121**, 247001 (2018).
[35] C. Zhang, J. Sous, D. R. Reichman, M. Berciu, A. J. Millis, N. V. Prokof'ev, and B. V. Svistunov, Bipolaronic High-Temperature Superconductivity, Phys. Rev. X **13**, 011010 (2023).
[36] B. Cohen-Stead, K. Barros, R. Scalettar, and S. Johnston, A hybrid Monte Carlo study of bond-stretching electron-phonon interactions and charge order in the bismuthate family of superconductors, npj Comput. Mater. **9**, 40 (2023).
[37] J. K. Freericks, M. Jarrell, and G. D. Mahan, The Anharmonic Electron-Phonon Problem, Phys. Rev. Lett. **77**, 4588 (1996).
[38] A. Chatterjee and Y. Takada, The Hubbard-Holstein model with anharmonic phonons in one dimension, J. Phys. Soc. Jpn. **73**, 964 (2004).
[39] C. P. J. Adolphs and M. Berciu, Going beyond the linear approximation in describing electron-phonon coupling: Relevance for the Holstein model, Europhys. Lett. **102**, 47003 (2013).
[40] S. Li and S. Johnston, The effects of non-linear electron-phonon interactions on superconductivity and charge-density-wave correlations, Europhys. Lett. **109**, 27007 (2015).
[41] S. Li, E. A. Nowadnick, and S. Johnston, Quasiparticle properties of the nonlinear Holstein model at finite doping and temperature, Phys. Rev. B **92**, 064301 (2015).
[42] P. M. Dee, J. Coulter, K. G. Kleiner, and S. Johnston, Relative importance of nonlinear electron-phonon coupling and vertex corrections in the Holstein model, Commun. Phys. **3**, 145 (2020).
[43] Ch. Uma Lavanya, I. V. Sankar, and A. Chatterjee, Metallicity in a Holstein-Hubbard chain at half filling with Gaussian anharmonicity, Sci. Rep. **7**, 3774 (2017).
[44] J. C. K. Hui and P. B. Allen, Effect of lattice anharmonicity on superconductivity, J. Phys. F **4**, L42 (1974).
[45] A. E. Karakozov and E. G. Maksimov, Influence of anharmonicity on superconductivity, Zh. Eksp. Teor. Fiz. **74**, 681 (1978) [Sov. Phys. JETP **47**, 358 (1978)].
[46] G. D. Mahan and J. O. Sofo, Resistivity and superconductivity from anharmonic phonons, Phys. Rev. B **47**, 8050 (1993).
[47] A. Szabó, S. A. Parameswaran, and S. Gopalakrishnan, High-temperature transport and polaron speciation in the anharmonic Holstein model, arXiv:2110.10170.
[48] J. Kondo, Localized atomic states in metals, Phys. B+C (Amsterdam) **84**, 40 (1976).
[49] T. Fuse and Y. Ōno, Rattling-induced heavy fermion state in the anharmonic Holstein model, J. Phys. Soc. Jpn. **80**, SA136 (2011).
[50] T. Fuse, Y. Ōno, and T. Hotta, Heavy-electron formation and polaron–bipolaron transition in the anharmonic Holstein model, J. Phys. Soc. Jpn. **81**, 044701 (2012).
[51] R. Blankenbecler, D. J. Scalapino, and R. L. Sugar, Monte Carlo calculations of coupled boson-fermion systems. I, Phys. Rev. D **24**, 2278 (1981).
[52] R. M. Noack and D. J. Scalapino, Green's-function self-energies in the two-dimensional Holstein model, Phys. Rev. B **47**, 305 (1993).
[53] M. Vekić, R. M. Noack, and S. R. White, Charge-density waves versus superconductivity in the Holstein model with next-nearest-neighbor hopping, Phys. Rev. B **46**, 271 (1992).
[54] F. Marsiglio, The spectral function of a one-dimensional Holstein polaron, Phys. Lett. A **180**, 280 (1993).
[55] G. G. Batrouni and R. T. Scalettar, Langevin simulations of a long range electron phonon model, Phys. Rev. B **99**, 035114 (2019).
[56] G. Paleari, F. Hébert, B. Cohen-Stead, K. Barros, R. T. Scalettar, and G. G. Batrouni, Quantum Monte Carlo study of an anharmonic Holstein model, Phys. Rev. B **103**, 195117 (2021).
[57] B. Cohen-Stead, O. Bradley, C. Miles, G. Batrouni, R. Scalettar, and K. Barros, Fast and scalable quantum Monte Carlo simulations of electron-phonon models, Phys. Rev. E **105**, 065302 (2022).
[58] Y. Zhang, C. Feng, R. Mondaini, G. G. Batrouni, and R. T. Scalettar, Charge singlets and orbital-selective charge density wave transitions, Phys. Rev. B **106**, 115120 (2022).
[59] G. G. Batrouni, G. R. Katz, A. S. Kronfeld, G. P. Lepage, B. Svetitsky, and K. G. Wilson, Langevin simulations of lattice field theories, Phys. Rev. D **32**, 2736 (1985).
[60] C. Chen, X. Y. Xu, J. Liu, G. Batrouni, R. Scalettar, and Z. Y. Meng, Symmetry-enforced self-learning Monte Carlo method applied to the Holstein model, Phys. Rev. B **98**, 041102(R) (2018).
[61] M. Yao, D. Wang, and Q.-H. Wang, Reducing autocorrelation time in determinant quantum Monte Carlo using the Wang-Landau algorithm: Application to the Holstein model, Phys. Rev. E **104**, 025305 (2021).
[62] A. B. Migdal, Interactions between electrons and lattice vibrations in a normal metal, Zh. Eksp. Teor. Fiz. **34**, 1438 (1958) [Sov. Phys. JETP **34**, 996 (1958)].
[63] G. M. Éliashberg, Interactions between electrons and lattice vibrations in a superconductor, Zh. Eksp. Teor. Fiz. **38**, 966 (1960) [Sov. Phys. JETP **11**, 696 (1960)].
[64] A. S. Alexandrov, Breakdown of the Migdal-Eliashberg theory in the strong-coupling adiabatic regime, Europhys. Lett. **56**, 92 (2001).
[65] E. D. Bauer, Y.-F. Yang, C. Capan, R. R. Urbano, C. F. Miclea, H. Sakai, F. Ronning, M. J. Graf, A. V. Balatsky, R. Movshovich, A. D. Bianchi, A. P. Reyes, P. L. Kuhns, J. D. Thompson, and Z. Fisk, Electronic inhomogeneity in a Kondo lattice, Proc. Natl. Acad. Sci. USA **108**, 6857 (2011).
[66] A. Auerbach and K. Levin, Kondo Bosons and the Kondo Lattice: Microscopic Basis for the Heavy Fermi Liquid, Phys. Rev. Lett. **57**, 877 (1986).
[67] H. Tsunetsugu, M. Sigrist, and K. Ueda, The ground-state phase diagram of the one-dimensional Kondo lattice model, Rev. Mod. Phys. **69**, 809 (1997).
[68] F. Steglich and S. Wirth, Foundations of heavy-fermion superconductivity: Lattice Kondo effect and Mott physics, Rep. Prog. Phys. **79**, 084502 (2016).
[69] M. A. Ruderman and C. Kittel, Indirect exchange coupling of nuclear magnetic moments by conduction electrons, Phys. Rev. **96**, 99 (1954).
[70] T. Kasuya, A theory of metallic ferro- and antiferromagnetism on Zener's model, Prog. Theor. Phys. **16**, 45 (1956).
[71] K. Yosida, Magnetic properties of Cu-Mn alloys, Phys. Rev. **106**, 893 (1957).

[72] M. Christensen, A. B. Abrahamsen, N. B. Christensen, F. Juranyi, N. H. Andersen, K. Lefmann, J. Andreasson, C. R. H. Bahl, and B. B. Iversen, Avoided crossing of rattler modes in thermoelectric materials, Nat. Mater. **7**, 811 (2008).

[73] G. S. Nolas, J. Poon, and M. Kanatzidis, Recent developments in bulk thermoelectric materials, MRS Bull. **31**, 199 (2006).

[74] N. Metropolis, A. W. Rosenbluth, M. N. Rosenbluth, A. H. Teller, and E. Teller, Equation of state calculations by fast computing machines, J. Chem. Phys. **21**, 1087 (1953).

[75] S. R. White, D. J. Scalapino, R. L. Sugar, E. Y. Loh, J. E. Gubernatis, and R. T. Scalettar, Numerical study of the two-dimensional Hubbard model, Phys. Rev. B **40**, 506 (1989).

[76] F. F. Assaad and H. G. Evertz, World-line and determinantal quantum Monte Carlo methods for spins, phonons and electrons, in *Computational Many-Particle Physics*, edited by H. Fehske, R. Schneider, and A. Weiße (Springer, Berlin, 2008), pp. 277–356.